

# Real-time effective-action approach to the Anderson quantum dot

Dénes Sexty, Thomas Gasenzer, and Jan Pawłowski

*Institut für Theoretische Physik, Ruprecht-Karls-Universität Heidelberg, Philosophenweg 16, 69120 Heidelberg, Germany and  
ExtreMe Matter Institute EMMI, GSI Helmholtzzentrum für Schwerionenforschung GmbH, Planckstraße 1, 64291 Darmstadt, Germany*  
(Dated: November 10, 2018)

The non-equilibrium time evolution of an Anderson quantum dot is investigated. The quantum dot is coupled between two leads forming a chemical-potential gradient. We use Kadanoff-Baym dynamic equations within a non-perturbative resummation of the s-channel bubble chains. The effect of the resummation leads to the introduction of a frequency-dependent 4-point vertex. The tunneling to the leads is taken into account exactly. The method allows the determination of the transient as well as stationary transport through the quantum dot, and results are compared with different schemes discussed in the literature (fRG, ISPI, tDMRG and QMC).

PACS numbers: 05.60.Gg 71.10.-w 73.63.Kv

## I. INTRODUCTION

Due to the recent advances in nanoscale technology, it has become possible to study electron transport experimentally in nano-devices such as single molecules, artificially designed quantum dots or nanotubes [1–5]. This naturally incited new interest, and quantum dot models have been the subject of much theoretical effort recently. The quantum dot also serves as a good playground for theoretical methods: it allows for many-body effects as well as non-equilibrium phenomena in a regime where linear response theory no longer applies. The description of co-tunneling processes such as the Kondo effect and the emergence of the Kondo scale have proven to be especially challenging. This is the case, in particular, for the exponential coupling dependence of the Kondo scale.

The Kondo regime has been investigated perturbatively using Fermi liquid theory [6], exploiting integrability of the Anderson model [7], or the non-crossing approximation at infinite local coupling  $U$  [8]. Several renormalization-group methods have been used to investigate the stationary state of the system: the perturbative real-time renormalization group (RG) [9], non-equilibrium extensions of perturbative RG [10–12], and the functional RG approach in its generalization to non-equilibrium situations [13–19]. Bethe-Salpeter equations in so-called parquet approximation [20] were analysed with respect to the Kondo resonance in Refs. [21–23]. The numerical renormalization group (NRG) method has also been successful in describing such impurity systems, and it has been generalized to describe time-dependent non-equilibrium systems [24–27].

Another line of thought is represented by the quantum Monte Carlo method (QMC) [28], which is numerically exact, but only short simulation times are possible since the method is plagued by the sign problem at small temperatures.

The transient behaviour of the system as well as the stationary state have also been explored by methods such as the time dependent density matrix renormalisation group (tDMRG) [29–32] which allows the simulation of the time evolution of pure states, and the iterative real-time summation of the path integral (ISPI) [33] which is numerically exact, but depends on the correlation time of the system being small. Several of these theoretical methods were recently compared in [34], which also contains a concise list of related previous studies.

In this article we use the two-particle-irreducible (2PI) effective action or  $\Phi$ -functional [35–37], to derive Kadanoff-Baym equations of motion describing the transient and stationary transport through a quantum dot. The power of this method is that symmetries of the system are conserved during the time evolution, i.e., particle number and energy conservation is satisfied. This method has been successfully applied to the thermalisation of relativistic and nonrelativistic systems of bosonic and fermionic gases [38–44].

We apply the 2PI method to the single-impurity Anderson model of a quantum dot within two different truncations: the loop expansion up to two-loop order (in the self-energy), and a resummation, which includes the contribution of the spin-aligned bubble chains summed to all orders. As shown below, the effect of this s-channel resummation can be seen as using a frequency dependent 4-point vertex. The leads can be taken into account exactly in this formalism: integrating them out they give a contribution to the self-energy of the dot-electrons.

After benchmarking our method against exact solutions for an isolated quantum dot we compare our results for the transient and stationary behavior of the dot coupled to the leads with results found in other schemes, including fRG, ISPI, tDMRG, and QMC calculations. While finding good agreement in the long-time stationary limit with the behavior found with these schemes our approach also allows to treat the transient build-up of the current through the dot. Comparisons of the stationary current for different interactions show good agreement with the alternative schemes over a large range of interaction strengths. These results underline the necessity of a nonperturbative resummation.

The structure of the paper is as follows: The Anderson model and its ingredients are defined in Section II. In Section III we summarize the formulation of the 2PI effective-action approach for nonrelativistic Fermions on an isolated quantum dot. We introduce the formulation for the dot coupled to leads in Section IV. In Section V we compare our method with exact results, for cases where an analytical treatment is possible. In Section VI we present our results for the build-up of the current and for its stationary characteristics, and compare these to results in the literature. We draw our conclusions in Section VII.

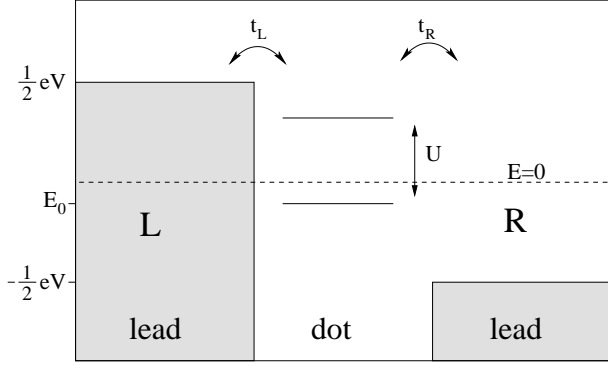


Figure 1: The schematic representation of the energy levels in the Anderson dot system, for the zero magnetic field case. The lower line of the dot represents the energy level of the first electron occupying the dot, the upper line is the level of the second electron occupying the dot.

## II. THE ANDERSON MODEL

The Anderson Hamiltonian describing the electrons on the quantum dot and on the leads reads

$$H = H_{\text{dot}} + H_{\text{leads}} + H_{\text{tunnel}} = \sum_{\sigma} E_{0\sigma} n_{\sigma} + U n_{\uparrow} n_{\downarrow} + \sum_{kp\sigma} \epsilon_{kp} c_{kp\sigma}^{\dagger} c_{kp\sigma} - \sum_{kp\sigma} (t_p c_{kp\sigma}^{\dagger} d_{\sigma} + t_p^* d_{\sigma}^{\dagger} c_{kp\sigma}) \quad (1)$$

where  $\sigma = \pm 1/2 \simeq \uparrow, \downarrow$  is the spin index,  $p = \pm \simeq L/R$  labels the leads on the left and right, respectively, and  $k$  is the index of the spectrum of the lead electrons. The leads on the left and right have a chemical potential  $\mu_p = peV/2$  which models the bias voltage. For the determination of the energies  $\epsilon_{kp}$ , see Sect. IV. The occupation-number operator on the dot is written as:  $n_{\sigma} = d_{\sigma}^{\dagger} d_{\sigma}$ . The dot electrons have an interaction term  $\sim U$  due to Coulomb repulsion. The one-body energy is  $E_{0\sigma} = E_0 + \sigma B$ . The first term is controlled experimentally through the gate voltage whereas the second (Zeeman) term by the magnetic field  $B$ . The energy levels of the system are represented in Fig. 1.

The tunneling between the dot and the leads is quantified by the tunneling strength  $t_p$ . We will assume that the leads are in thermal equilibrium at some temperature  $T$  and use the usual wide-band limit with a constant density of states  $\rho$  around the Fermi surface. In this work we use a symmetric tunneling rate  $\tau = t_L = t_R$ . The dimensionful quantities of the system can be expressed in units of the hybridization  $\Gamma = 2\pi|\tau|^2\rho$  which quantifies the dressing of the dot by the leads.

We will use, in the following, a Lagrangian or action formulation of the Anderson quantum field model. The contributions to the action corresponding to those forming the Hamil-

tonian (1) are given by

$$S_{\text{dot}} = \int_C dt \sum_{\sigma} d_{\sigma}^{\dagger} (i\partial_t - E_{0\sigma}) d_{\sigma} - U d_{\uparrow}^{\dagger} d_{\uparrow} d_{\downarrow}^{\dagger} d_{\downarrow}, \quad (2)$$

$$S_{\text{leads}} = \int_C dt \sum_{kp\sigma} c_{kp\sigma}^{\dagger} (i\partial_t - \epsilon_{kp}) c_{kp\sigma}, \quad (3)$$

$$S_{\text{tunnel}} = \int_C dt \sum_{kp\sigma} (t_p c_{kp\sigma}^{\dagger} d_{\sigma} + t_p^* d_{\sigma}^{\dagger} c_{kp\sigma}). \quad (4)$$

Our most important observable is the time dependent current through the dot

$$I(t) = -\frac{ie}{2} \sum_{kp\sigma} \left( p t_p \langle c_{kp\sigma}^{\dagger} d_{\sigma} \rangle - p t_p^* \langle d_{\sigma}^{\dagger} c_{kp\sigma} \rangle \right). \quad (5)$$

This can also be written as  $I = (I_L - I_R)/2$ , where  $I_p = -e\dot{N}_p(t)$  and  $N_p(t) = \langle \sum_{k\sigma} c_{kp\sigma}^{\dagger} c_{kp\sigma} \rangle$  the number of electrons on the leads. The stationary current can simply be obtained by waiting for the transient behavior to die out, such that the system is sufficiently close to the final, stationary state.

An important scale of the physical processes described by the Anderson model is given by the Kondo temperature. This temperature marks the onset of the Kondo effect which is due to the formation of singlet states of itinerant and localised dot fermions and characterised by a rising resistivity of the dot at low temperatures. The Kondo temperature is found by simple renormalisation-group arguments to be

$$T_K = \sqrt{\frac{U\Gamma}{2}} \exp\left(\frac{-\pi U}{8\Gamma}\right). \quad (6)$$

for the particle-hole symmetric system, where  $E_0 = -U/2$ .

## III. 2PI FORMALISM FOR THE ISOLATED DOT

In this paper, we study Kadanoff-Baym-type dynamic equations for correlation functions describing transport through the Anderson quantum dot. We derive these equations using the two-particle irreducible (2PI) effective-action formalism, also known as  $\Phi$ -derivable approach. In the following, we summarize known basics about the 2PI effective-action approach [35–37] and introduce specific details of its implementation for the Anderson model.

Since we will be interested in initial value problems, specifically, in the evolution of multi-time correlation functions starting from values given by some initial state, it is convenient to work in the Heisenberg picture. In the corresponding functional-integral formulation, the time integrations in the action are defined to run along a Schwinger-Keldysh contour  $C$ , which goes from the initial time  $t_0$  to some final time  $t$ , and then back to  $t_0$  [45, 46].

The Kadanoff-Baym equations will yield the evolution of the time-ordered two-point function:

$$D_{\sigma\lambda}(t, t') = \Theta_C(t - t') \langle d_{\sigma}(t) d_{\lambda}^{\dagger}(t') \rangle - \Theta_C(t' - t) \langle d_{\lambda}^{\dagger}(t') d_{\sigma}(t) \rangle \quad (7)$$

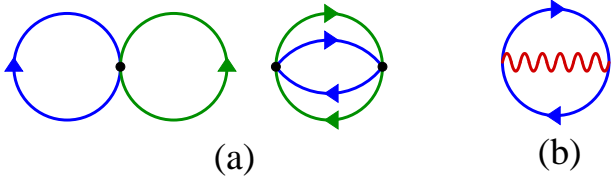


Figure 2: (color online) 2PI diagrams of the loop expansion of  $\Gamma_2[D]$ . (a) The two lowest-order diagrams of the loop expansion described in sections III A and III B, with each vertex coupling up spins to down spins. Black dots represent the bare vertex  $\sim U$ , blue (green) solid lines the up (down) spin propagator  $D_{\sigma\sigma}$ ,  $\sigma = \uparrow, \downarrow$ . (b) Diagram representing the resummation approximation explained in Sect. III C. The wiggly line is the scalar approximation  $G_{11}$ . This propagator is represented as a sum of bubble-chain diagrams, see (35). The same diagram with down spins also appears in  $\Gamma_2[D]$ .

where  $\Theta_C(t - t')$  is a  $\Theta$ -function on the Schwinger-Keldysh contour, and evaluates to 1 (0) if  $t$  is later (earlier) to  $t'$ .

We begin with the simpler case of the isolated quantum dot. Without leads the 2PI effective action [37] reads

$$\Gamma[D] = -i\text{Tr}[\ln D^{-1} + D_0^{-1}D] + \Gamma_2[D] + \text{const.} \quad (8)$$

Here  $\Gamma_2[D]$  can be written as the sum of all closed 2PI diagrams constructed from bare vertices and full propagators. Two-particle irreducible are those diagrams which do not fall apart upon cutting two lines [37]. As an example we show, in Fig 2a, the two diagrams of lowest order in the bare coupling  $U$ , represented as a black dot. Full lines denote different spin components of the full propagator or two-point function  $D$ . In (8), the free inverse propagator is given by

$$iD_{0,\sigma\lambda}^{-1}(t, t') = (i\partial_t - E_{0\sigma})\delta_C(t - t')\delta_{\sigma\lambda}. \quad (9)$$

The Kadanoff-Baym equations of motion are calculated from the stationarity conditions for the action

$$\frac{\delta\Gamma[D]}{\delta D_{\lambda\sigma}(t', t)} = 0. \quad (10)$$

This equation gives the well-known Dyson equation  $D_{\sigma\lambda}^{-1}(t, t') = D_{0,\sigma\lambda}^{-1}(t, t') - \Sigma_{\sigma\lambda}(t, t')$ , where the self-energy is given by

$$\Sigma_{\sigma\lambda}(t, t') = -i \frac{\delta\Gamma_2[D]}{\delta D_{\lambda\sigma}(t', t)}. \quad (11)$$

We use the decomposition of the time-ordered two-point function (7)

$$D_{\sigma\lambda}(t, t') = F_{\sigma\lambda}(t, t') - \frac{i}{2}\rho_{\sigma\lambda}(t, t')\text{sign}_C(t - t'), \quad (12)$$

where

$$\begin{aligned} F_{\sigma\lambda}(t, t') &= \frac{1}{2}\langle [d_\sigma(t), d_\lambda^\dagger(t')] \rangle, \\ \rho_{\sigma\lambda}(t, t') &= i\langle \{d_\sigma(t), d_\lambda^\dagger(t')\} \rangle, \end{aligned} \quad (13)$$

are the so-called statistical and spectral correlation functions in real-time representation.  $\text{sign}_C(t - t') = -1 + 2\Theta_C(t - t')$  is a sign function on the contour. For the equal-time arguments the following identities hold

$$F_{\sigma\sigma}(t, t) = \frac{1}{2} - n_\sigma(t), \quad \rho_{\sigma\lambda}(t, t) = i\delta_{\sigma\lambda} \quad (14)$$

where  $n_\sigma(t)$  is the mean number of fermions occupying the dot level with spin  $\sigma$  at time  $t$  and the equation for  $\rho(t, t')$  follows from the fermionic equal-time anticommutation relations. The symmetry relations

$$F_{\sigma\lambda}(t, t') = F_{\lambda\sigma}(t', t)^*, \quad \rho_{\lambda\sigma}(t, t') = -\rho_{\sigma\lambda}(t', t)^*. \quad (15)$$

are a direct consequence of the definitions of  $F$  and  $\rho$ . For its numerical solution it is convenient to rewrite the Dyson equation for  $D(t, t')$  in terms of two equations for  $F(t, t')$  and  $\rho(t, t')$  whereby the time integrals over the contour  $C$  are replaced by simple integrations along the real-time axis. In this way one arrives at the usual 2PI or Kadanoff-Baym equations of motion for the complex functions  $F(t, t')$  and  $\rho(t, t')$ .

We will assume throughout that correlations between up and down spins vanish, such that  $D_{\sigma\lambda} \sim \delta_{\sigma\lambda}$ . We also introduce the notation:  $D_{\sigma\sigma} \equiv D_\sigma$  (no summation!). With this, the equations of motion read

$$\begin{aligned} (i\partial_t - M_\sigma(t))\rho_\sigma(t, t') &= \int_{t'}^t du \Sigma_\sigma^p(t, u)\rho_\sigma(u, t'), \\ (i\partial_t - M_\sigma(t))F_\sigma(t, t') &= \int_0^{t'} du \Sigma_\sigma^p(t, u)F_\sigma(u, t') \\ &\quad - \int_0^{t'} du \Sigma_\sigma^F(t, u)\rho_\sigma(u, t'), \end{aligned} \quad (16)$$

where the decomposition

$$\begin{aligned} \Sigma_\sigma(t, t') &= -i\Sigma_\sigma^{(0)}(t)\delta(t - t') + \\ &\quad + \Sigma_\sigma^F(t, t') - \frac{i}{2}\text{sign}_C(t - t')\Sigma_\sigma^p(t, t'). \end{aligned} \quad (17)$$

of the self-energy into local,  $F$  and  $\rho$  type terms has been used. The time-local energy term in (16) is given by

$$M_\sigma(t) = E_{0\sigma} + \Sigma_\sigma^{(0)}(t) \quad (18)$$

and includes the mean-field shift originating from the double-bubble diagram in Fig 2a. The above integro-differential equations are equivalent to the exact Kadanoff-Baym equations and include higher-order correlations through the non-Markovian memory integrals on their right hand side.

Including the second-order ‘basket-ball’ diagram in Fig 2a beyond the mean-field approximation yields a perturbative small-coupling approximation of  $\Gamma_2[D]$ ,

$$\begin{aligned} \Gamma_2[D] &= -U \int_C dt D_\uparrow(t, t)D_\downarrow(t, t) \\ &\quad + \frac{i}{2}U^2 \int_C dt dt' D_\uparrow(t, t')D_\uparrow(t', t)D_\downarrow(t, t')D_\downarrow(t', t). \end{aligned} \quad (19)$$

In the self-energy this corresponds to taking into account the tadpole and sunset diagrams.

### A. Mean-field approximation

The one-loop contribution to the self-energy gives the mean-field approximation of the dynamic equations (16),

$$\Sigma_{\sigma}^{MF}(t, t') = iU\delta(t - t')D_{-\sigma}(t, t'). \quad (20)$$

Note that  $D_{\sigma}(t, t')$  has a jump at equal time arguments. By analyzing the path-integral construction one finds that using the specific operator ordering in the Hamiltonian (A2) implies that the self-energy takes the form

$$\Sigma_{\sigma}^{MF}(t, t') = -iUn_{-\sigma}\delta(t - t'). \quad (21)$$

See Appendix A for details. The resulting equations of motion to this order of approximation are local in time and therefore Markovian. They constitute the 1-loop or mean-field approximation.

### B. Second-order approximation

We finally derive the order- $U^2$  contribution to the self energies, also called second-order Born approximation,

$$\Sigma_{\sigma}^{\text{Sunset}}(t, t') = U^2 D_{\sigma}(t, t') D_{-\sigma}(t, t') D_{-\sigma}(t', t), \quad (22)$$

or, in components,

$$\begin{aligned} \Sigma_{\sigma}^F &= U^2 \left[ F_{\sigma} \left( |F_{-\sigma}|^2 - \frac{1}{4} |\rho_{-\sigma}|^2 \right) \right. \\ &\quad \left. - \frac{1}{4} \rho_{\sigma} (F_{-\sigma} \rho_{-\sigma}^* + F_{-\sigma}^* \rho_{-\sigma}) \right], \\ \Sigma_{\sigma}^{\rho} &= U^2 \left[ \rho_{\sigma} \left( |F_{-\sigma}|^2 - \frac{1}{4} |\rho_{-\sigma}|^2 \right) + \right. \\ &\quad \left. + F_{\sigma} (F_{-\sigma} \rho_{-\sigma}^* + F_{-\sigma}^* \rho_{-\sigma}) \right] \end{aligned} \quad (23)$$

where we have omitted arguments. The contributions (21) and (23) are summed up to be used in Eq. (16), with (21) contributing to  $\Sigma_{\sigma}^{(0)}$ . Some details concerning the numerical implementation of the above equations are given in App. B.

### C. s-channel resummation

In this section we will summarize the  $s$ -channel resummation which leads substantially beyond the coupling approximations discussed before. Specifically, this involves a summation of the bubble chain contributions with alternating spins where, in each bubble, the two propagators describe the same spin component. This is similar to the next-to-leading-order  $1/N$  approximation for  $N$ -component scalar fields [38, 49]. An elegant way to perform the resummation involves a Hubbard-Stratonovich (HS) transformation. Since the interaction vertex couples 'up' spins with 'down' spins, the bubbles in the chain have alternating spins. The action

$$S_{\text{dot}} = \int_C dt \sum_{\sigma} d_{\sigma}^{\dagger} (i\partial_t - E_{0\sigma}) d_{\sigma} - U d_{\uparrow}^{\dagger} d_{\uparrow} d_{\downarrow}^{\dagger} d_{\downarrow} \quad (24)$$

is rewritten using auxiliary scalar fields  $\chi_1$  and  $\chi_2$  by use of the substitution

$$-JA^{-1}J \rightarrow \chi_T A \chi + 2J_T \chi \quad (25)$$

where

$$J = \frac{1}{2} \begin{pmatrix} d_{\uparrow}^{\dagger} d_{\uparrow} \\ d_{\downarrow}^{\dagger} d_{\downarrow} \end{pmatrix}, \quad \chi = \begin{pmatrix} \chi_1 \\ \chi_2 \end{pmatrix}, \quad A = \frac{1}{2U} \begin{pmatrix} 0 & 1 \\ 1 & 0 \end{pmatrix}.$$

The resulting action reads

$$\begin{aligned} S_{\text{dot}}[d_{\sigma}, d_{\sigma}^{\dagger}, \chi_i] &= \int_C dt \sum_{\sigma} d_{\sigma}^{\dagger} (i\partial_t - E_{0\sigma}) d_{\sigma} \\ &\quad + \frac{1}{U} \chi_1 \chi_2 + d_{\uparrow}^{\dagger} d_{\uparrow} \chi_1 + d_{\downarrow}^{\dagger} d_{\downarrow} \chi_2. \end{aligned} \quad (26)$$

The free inverse propagators are read off from the quadratic part of the action

$$\begin{aligned} iG_0^{-1}(t, t') &= 2A\delta(t - t'), \\ iD_{0,\sigma}^{-1}(t, t') &= (i\partial_t - E_{0\sigma} + \bar{\chi}_i)\delta(t - t') \end{aligned} \quad (27)$$

where the free propagator  $G_0$  of the scalar fields is a  $2 \times 2$  matrix. Accordingly, we call  $G$  the propagator of the scalars, and  $\bar{\chi}_i$  is the one-point function or expectation value of the auxiliary fields.

The corresponding 2PI effective action can be written as:

$$\begin{aligned} \Gamma[G, D, \bar{\chi}] &= S_{\text{dot}}[d_{\sigma}^{\dagger} = d_{\sigma} = 0, \bar{\chi}] - i\text{Tr} [\ln D^{-1} + D_0^{-1} D] \\ &\quad + \frac{i}{2} \text{Tr} [\ln G^{-1} + G_0^{-1} G] + \Gamma_2[D, G] + \text{const.} \end{aligned} \quad (28)$$

where  $\Gamma_2[D, G]$  contains all closed 2PI diagrams built from the 3-point vertices of the action (26) and full scalar and fermion propagators. The lowest-order contribution is shown in Fig. 2b.

The stationarity conditions give the Schwinger-Dyson equations. In this case, the field average of the scalar fields, in contrast to that of the fermionic fields, is nonzero, so we have stationary equations of the form  $\delta\Gamma/\delta\bar{\chi} = 0$ . The resulting equations read

$$\bar{\chi}_1(t) = UD_{\downarrow\downarrow}(t, t), \quad \bar{\chi}_2(t) = UD_{\uparrow\uparrow}(t, t), \quad (29)$$

$$D_0^{-1}D = \Sigma * D + \delta, \quad (30)$$

$$G_0^{-1}G = \Pi * G + \delta \quad (31)$$

where we again suppressed the time arguments, and  $*$  stands for convolution on the contour  $C$ ,

$$(A * B)(t, t') = \int_C dz A(t, z) B(z, t'). \quad (32)$$

$\Sigma$  and  $\Pi$  are the self-energy of the fermion and the boson fields, respectively:

$$\begin{aligned} \Sigma_{\sigma}(t, t') &= -i \frac{\partial \Gamma_2[D, G]}{\partial D_{\sigma}(t', t)} = -D_{\sigma}(t, t') G_{\sigma\sigma}(t, t'), \\ \Pi(t, t') &= 2i \frac{\partial \Gamma_2[D, G]}{\partial G(t, t')}, \\ \Pi_{\sigma\sigma} &= D_{\sigma}(t, t') D_{\sigma}(t', t), \quad \Pi_{12} = \Pi_{21} = 0 \end{aligned} \quad (33)$$

where  $\uparrow = 1$ ,  $\downarrow = 2$  is used for the field indices.

The equations concerning the scalar fields are constraint equations, which do not contain any time derivatives, because the  $\chi$  fields are auxiliary, non-dynamical fields. The  $\Gamma_2$  part of the action to lowest order is obtained as (See Fig. 2b)

$$\Gamma_2[D, G] = -\frac{i}{2} \sum_{\sigma} \int D_{\sigma}(x, y) D_{\sigma}(y, x) G_{\sigma\sigma}(x, y). \quad (34)$$

From the constraint equation (31) for  $G$ , one can see that

$$\begin{aligned} G = & iU\delta \begin{pmatrix} 0 & 1 \\ 1 & 0 \end{pmatrix} - U^2 \begin{pmatrix} \Pi_{22} & 0 \\ 0 & \Pi_{11} \end{pmatrix} \\ & - iU^3 \begin{pmatrix} 0 & \Pi_{22} * \Pi_{11} \\ \Pi_{11} * \Pi_{22} & 0 \end{pmatrix} \\ & + U^4 \begin{pmatrix} \Pi_{22} * \Pi_{11} * \Pi_{22} & 0 \\ 0 & \Pi_{11} * \Pi_{22} * \Pi_{11} \end{pmatrix} + \dots, \end{aligned} \quad (35)$$

where we have again omitted the  $(t, t')$  arguments. Inserting  $G_{11}$  and  $G_{22}$  into the self-energy  $\Sigma$  of the fermions in eq. (33), one finds a sum of bubble chains with alternating spins being generated as mentioned initially. The decomposition of the propagator  $G$  and the self energies into statistical and spectral parts is deferred to Appendix C.

#### IV. LEADS IN THE 2PI FORMALISM

In this section we couple the single dot system to the leads taking into account the terms (3) and (4) in the action. We can calculate the leads' contribution exactly, since (3) and (4) only include terms up to quadratic order, by integrating these out. The initial density matrix of the full system is assumed to be of the product form

$$\rho(t=0) = \rho_{\text{dot}} \otimes \rho_{\text{leads}}, \quad (36)$$

i.e., no correlations between dot and lead electrons exist initially.  $\rho_{\text{dot}}$  is described in Sect. V A, while  $\rho_{\text{leads}}$  describes a grand-canonical ensemble, as shown below. To include a thermal density matrix for the lead electrons, we expand their time-contour with a vertical part after  $C$  from  $t_0$  to  $t_0 - i\beta$  for each momentum mode of the lead electrons. Then, the contribution to the dot degrees of freedom is

$$iS_{\text{env}} = -i|\tau|^2 \int_C dt dt' d^\dagger(t) S^{-1}(t, t') d(t') \quad (37)$$

where  $S(t, t')$  is the free action of the lead electrons,

$$S(t, t') = (i\partial_t - \epsilon(t))\delta(t - t'). \quad (38)$$

Note that we have chosen symmetric tunneling  $\tau = t_L = t_R$ . Here  $t$  is a complex variable, which lives on the extended Schwinger-Keldysh contour.  $\epsilon(t) = \epsilon_{kp}$  if  $t$  is real, with  $k$  and  $p$  being the indices of the mode considered, and  $\epsilon(t) = \epsilon_{kp} - \mu$  if  $t$  is on the vertical part of the contour. This prescription gives the correct initial density matrix corresponding to the grand canonical ensemble.

To obtain the contribution to  $S_{\text{env}}$ , we have to solve the equation

$$(i\partial_t - \epsilon(t))A(t, t') = \delta_C(t, t'), \quad (39)$$

using the antiperiodic boundary condition  $A(0, t') = -A(-i\beta, t')$ . The result can be written in the form

$$\begin{aligned} S^{-1}(t, t') &= A(t, t') \\ &= A^>(t, t')\Theta_C(t - t') - A^<(t, t')\Theta_C(t' - t), \end{aligned} \quad (40)$$

$$\begin{aligned} A^>(t, t') &= -i(1 - f(\epsilon_{kp} - \mu))e^{-i\epsilon_{kp}(t - t')}, \\ A^<(t, t') &= -if(\epsilon_{kp} - \mu)e^{-i\epsilon_{kp}(t - t')} \end{aligned} \quad (41)$$

where  $f(x) = 1/[1 + \exp(\beta x)]$  is the Fermi function. After integrating the lead electrons out, this appears as part of the free propagator of the dot electrons, so we have

$$[D_0^{-1} + iA] * D = \Sigma * D + \delta. \quad (42)$$

After decomposition one finds that the effect of one lead-electron mode can be seen as a contribution to the self-energy of the dot electrons  $\Sigma^F$  and  $\Sigma^\rho$ :

$$\Sigma_{\text{lead}}^{F(1)}(t, t') = -|\tau|^2 \left( \frac{1}{2} - f(\epsilon - \mu) \right) e^{-i\epsilon(t - t')}, \quad (43)$$

$$\Sigma_{\text{lead}}^{\rho(1)}(t, t') = -i|\tau|^2 e^{-i\epsilon(t - t')}. \quad (44)$$

One can also argue the following way: If the tunneling terms are used as a vertex, they give a one-loop diagram in  $\Gamma_2[D]$ , half of the loop is the propagator of the electron on the dot, the other half is the propagator of the lead-electron. After taking the derivative of  $\Gamma[D]$  one sees that up to a factor the contribution to the self-energy is the propagator of the free lead electron. This gives the same result as above.

Hence, the contribution only depends on the difference of the time arguments. This is to be expected, since the lead electrons are in thermal equilibrium. Now we have the contribution of one lead particle. The wide-band limit corresponds to integrating over a continuum

$$\Sigma_{\text{lead}} = \int_{-D}^D d\epsilon \rho(\epsilon) \Sigma_{\text{lead}}^{(1)} \quad (45)$$

with  $\rho(\epsilon) = \text{const}$ . With (44) this leads to

$$\Sigma_{\text{lead}}^\rho = - \int_{-D}^D d\epsilon i|\tau|^2 e^{-i\epsilon t} = -i|\tau|^2 2 \frac{\sin Dt}{t}. \quad (46)$$

It is useful to consider the limit  $D \rightarrow \infty$ , where

$$\Sigma_{\text{lead}}^\rho(t, t') = -2i\pi|\tau|^2 \delta(t - t'). \quad (47)$$

The calculation of  $\Sigma^F$  can only be done analytically at zero temperature. The finite-temperature correction is calculated numerically, whereas the zero-temperature contribution is a principal value,

$$\Sigma_{\text{lead}, T=0}^F(t) = i|\tau|^2 P \frac{e^{-i\mu t}}{t} = \sum_{L,R} \lim_{\epsilon \rightarrow 0} i|\tau|^2 e^{-i\mu t} \frac{t}{t^2 + \epsilon^2}. \quad (48)$$

To calculate the time dependent non-equilibrium current, one adds a further source term to the action:

$$S_\eta = \frac{i\eta}{2} \sum_{kp\sigma} p(t_p c_{kp\sigma}^\dagger d_\sigma - t_p^* d_\sigma^\dagger c_{kp\sigma})(t_m) \quad (49)$$

Then the current at some measurement time  $t_m$  can be written as

$$I(t_m) = -i \frac{\partial}{\partial \eta} \ln Z[\eta] \Big|_{\eta=0}. \quad (50)$$

After integrating out the leads, one gets the following contribution to the action:

$$iS_{\text{lead}} = -i \sum_p \int_C dt \int_C dt' d^\dagger(t) \left\{ A_p(t, t') + \frac{i\eta}{2} A_p(t, t') [-\delta(t - t_m) + \delta(t' - t_m)] \right\} d(t') \quad (51)$$

where we dealt with the first term in the previous subsection, see Eq. (40). The second term will provide a contribution to the current which thus reads

$$I_L(t) = e \sum_\sigma \int_0^{t_m} dt \left[ A_L^F(t_m, t) \rho_\sigma(t, t_m) - A_L^\rho(t_m, t) F_\sigma(t, t_m) + A_L^{F*}(t_m, t) \rho_\sigma^*(t, t_m) - A_L^{\rho*}(t_m, t) F_\sigma^*(t, t_m) \right]. \quad (52)$$

For the full current one needs  $I = (I_L - I_R)/2$ . If the leads are symmetric (tunneling rate, temperature and level density are the same for the left and the right lead) the  $A_p$  terms cancel,

$$I_{\text{symm}} = e \text{Re} \sum_\sigma \int_0^{t_m} dt \left[ A_L^F(t_m, t) - A_R^F(t_m, t) \right] \rho_\sigma(t, t_m). \quad (53)$$

## V. COMPARISON WITH EXACT RESULTS

### A. Exact time evolution without leads

Without the leads, the time evolution of the dot is a simple quantum-mechanics problem of solving the Schrödinger equation. To compare with results obtained with the above functional methods, we need to choose an initial density matrix for which the 1-point, 3-point and higher connected  $n$ -point functions are zero:  $\text{Tr}(\rho d_\sigma) = 0$ ,  $\text{Tr}(\rho d_\sigma d_{-\sigma}^\dagger d_{-\sigma}) = 0$ ,  $\text{Tr}(\rho F_{\sigma\lambda}) = \delta_{\sigma\lambda}(1/2 - n_\sigma)$ ,  $\text{Tr}(\rho d_\sigma d_{-\sigma}) = 0$ , etc. These requirements fully constrain the density matrix.

Then one can solve the time evolution analytically by diagonalizing  $H_{\text{dot}}$  defined in Eq. (1). The commutator part of the 2-point function is given by

$$F_{11}(0, t) = F_{11}^*(t, 0) = \frac{1}{2} \left[ (1 - n_1)(1 - n_2) e^{iE_0 t} + (1 - n_1)n_2 e^{i(E_0 + U)t} - n_1(1 - n_2) e^{iE_0 t} - n_1 n_2 e^{i(E_0 + U)t} \right]. \quad (54)$$

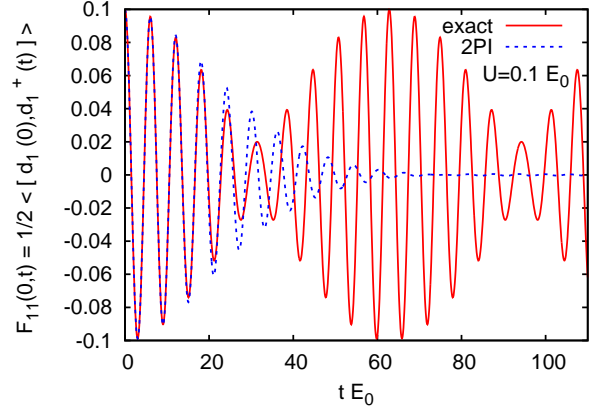


Figure 3: Time evolution of the two-time correlation function  $F_{11}(0, t)$  for an isolated quantum dot: Comparison of 2PI and exact results obtained by directly solving the Schrödinger equation. The magnetic field is zero. While the exact evolution shows revivals, the oscillations are damped out within the 2PI approach.

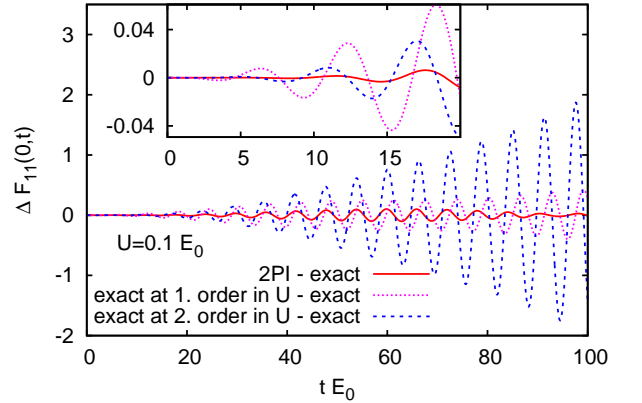


Figure 4: The same time evolution as in Fig. 3: Comparison of 2PI and exact results. The difference between the exact and 2PI results, as well as the difference between the Taylor-expanded exact and the exact results are shown.

We compare this non-equal-time two-point function to the solution of the Kadanoff-Baym equations obtained from the 2PI effective action. As one sees in Fig. 3, the 2PI solution is in good agreement in the beginning, but does not show revivals as expected, cf., e.g., Refs. [50, 51]. Coupling to the leads causes a real damping which the 2PI approach is capable to describe. In Fig. 4 we plot the difference between the exact and the 2PI results for  $F_{11}(0, t)$ , as well as the difference between the exact and the Taylor-expanded exact results. This illustrates that the 2PI equations yield a well-behaved dynamics. In contrast to this, perturbation theory shows secularity problems.

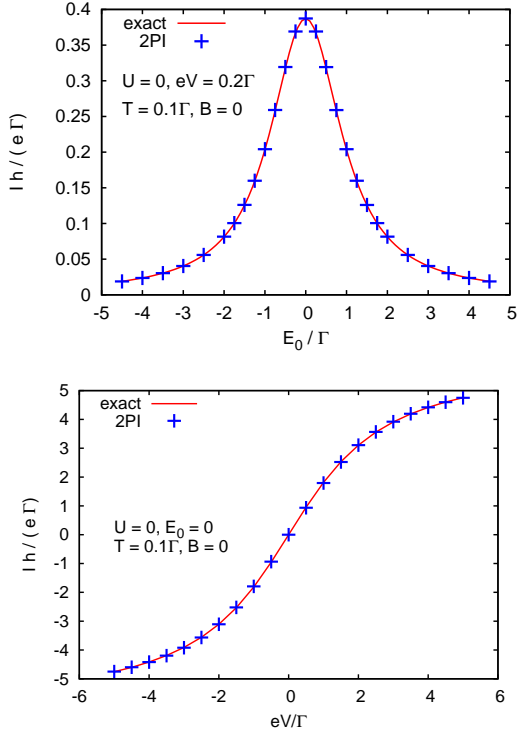


Figure 5: The stationary current (55) through the quantum dot at  $U = 0$ , as a function of the bias voltage. The comparison of the 2PI results and the results of Ref. [14], which in this case are both exact, serves as a benchmark test.

### B. The current at $U = 0$

Another quantity which can be calculated exactly is the current at vanishing on-dot coupling  $U$ . This is due to the fact that at zero coupling the dot degrees of freedom are also quadratic. For details of the calculation, see, e.g., Ref. [14]. The result is

$$I = \frac{1}{\pi} \int d\epsilon (f(\epsilon - \mu_L) - f(\epsilon - \mu_R)) \frac{\Gamma^2}{(\omega - E_0)^2 + \Gamma^2} \quad (55)$$

where  $f(x) = 1/[1 + \exp(\beta x)]$  is the Fermi function.

In Fig. 5, the currents as obtained from the analytical formula (55) and from the 2PI calculation (after waiting for the stationary state), for  $U = 0$ , are compared. The agreement benchmarks our calculation, because we take the leads into account exactly, and at  $U = 0$  the 2PI treatment is also exact.

## VI. TRANSIENT AND STATIONARY DYNAMICS

In the remainder of this paper we present our results for the transient build-up of the current through the quantum dot, for different coupling strengths, bias voltages, and temperatures. We compare our results with those obtained with alternative methods as given in the literature. As we will show, these underline the necessity to go beyond the perturbative coupling expansion of the 2PI part  $\Gamma_2$  of the effective action. Our results

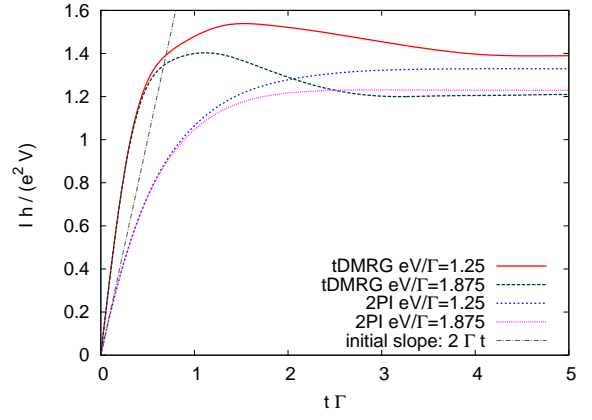


Figure 6: Comparison of the transient currents obtained with the 2PI equations and with the tDMRG method, at the symmetric point:  $E_0 = -U/2$ . The parameters are:  $U = 3\Gamma, T = 0.1\Gamma$ . Note that the different initial slopes are due to differently chosen initial conditions. While, in the tDMRG calculation, initial correlations between dot and leads are present, there are no such correlations in the 2PI approach.

also give hints to the limitations of the  $s$ -channel resummation. We consider first the transient evolution of the current, showing the build-up of the stationary state and then analyse the resulting asymptotic current.

### A. Numerical comparisons of different approaches

For the comparisons we use data that was published in Refs. [33, 34]. For details about the fRG (functional Renormalisation Group), ISPI (Iterative Summation of real-time Path Integrals), QMC (Quantum Monte Carlo) and tDMRG (time-dependent Density Matrix Renormalization Group), see, e.g., Ref. [34], and references therein. If not otherwise stated, we will use the particle-hole symmetric point, where  $E_0 = -U/2$ , and  $U = 2\Gamma, B = 0, T = 0.1\Gamma$ .

In Fig. 6 we compare the time dependence of the current through the dot as obtained with the full 2PI equations of motion with the results of the tDMRG method. The stationary values obtained with the two methods are close to each other, but the time dependences are different. The initial slope of the current for the 2PI curve is given by  $Ih/(e^2 V) = 2\Gamma t$ , as can be seen by evaluating the Heisenberg equation of motion  $\dot{I} = i/\hbar [H, I]$ , with the uncorrelated density matrix (36) at the initial time. The tDMRG method uses an initial density matrix containing correlations between dot and lead electrons, which explains the different slope at the initial time.

In Fig. 7 we compare, for small couplings, the stationary current with the corresponding results of the ISPI approach discussed in Ref. [33]. The perturbative results were presented in Ref. [52]. Note that we plot the interaction correction, that is, the difference of the currents for zero and non-zero coupling which, for the chosen couplings, is a small quantity. The Coulomb-blockade physics suggests that the sign of the cor-

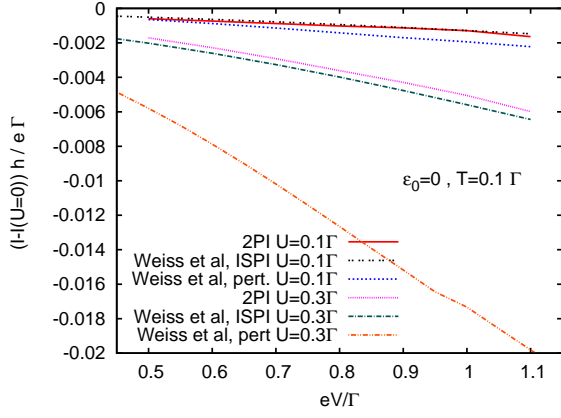


Figure 7: The modification of the asymptotic stationary current due to nonvanishing interactions is shown as functions of the bias voltage. The results obtained with the 2PI method are compared with those of the ISPI calculations given in Ref. [33], and with perturbative results from Ref. [52].

rection should be negative, as transport is suppressed for non-degenerate levels on the dot. One observes that the agreement between the results of the two methods, within the range of couplings considered, is very good. For  $U = 0.1\Gamma$  the perturbative results are close to the ISPI and 2PI results. We find that for  $U = 0.3\Gamma$  the perturbation theory is of limited accuracy while the 2PI and ISPI results agree well.

In Fig. 8 the time dependence of the current is shown for different choices of the interaction, the bias voltage, and the temperature. We compare the second-order coupling expansion, see Sect. III B, with the  $s$ -channel resummation introduced in Sect. III C. For the case of stronger interactions we compare the stationary current reached with the result obtained with perturbative RG methods, as given in Ref. [33]. While for small coupling the truncations agree and reproduce the ISPI result given in Ref. [33], deviations appear for larger  $U$ , where the system is expected to enter the Kondo regime.

In Fig. 9 we compare the stationary current for bigger couplings, at the particle-hole symmetric point ( $E_0 = -U/2$ ), with corresponding results from the other methods. With this we provide an add-on to the comparison presented in Ref. [34]. One finds that for  $U = 2\Gamma$  all methods agree. At  $U = 4\Gamma$  deviations start to appear which become larger at  $U = 8\Gamma$ .

In Fig. 10 we test the mixed-valence regime, by comparing the steady-state current, using  $E_0 = \Gamma = -U/2 + 2\Gamma$ . For small bias voltages one sees good agreement between all methods. For further details concerning the other methods see the discussion in Ref. [31]. We furthermore compare our results with those from the fRG and ISPI methods at non-zero magnetic field, as shown in Fig. 11, and find good agreement for the full range of bias voltages. In Fig. 12 we finally compare the temperature dependence of the steady-state current with fRG and ISPI results, for  $U = 2\Gamma$ ,  $T = 0.1\Gamma$ . One finds good agreement for all three methods, with the largest deviations in the high-temperature large-bias regime.

Overall, we conclude that in the moderate-coupling re-

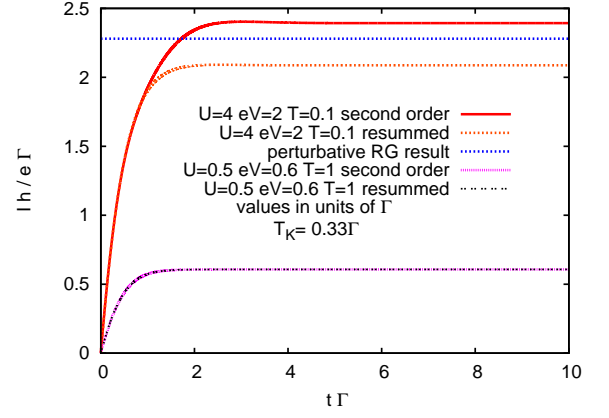


Figure 8: The time dependent current through the dot is shown for different couplings  $U$ , bias voltage  $V$ , and temperature  $T$ . We compare results obtained within the second-order truncation of the 2PI effective action with those derived after  $s$ -channel resummation. For  $U = 2\Gamma$  there is perfect agreement. Note that, for the bigger coupling, the Kondo temperature (6) is  $T_K = 0.33\Gamma$  such that the system is already in the Kondo regime.

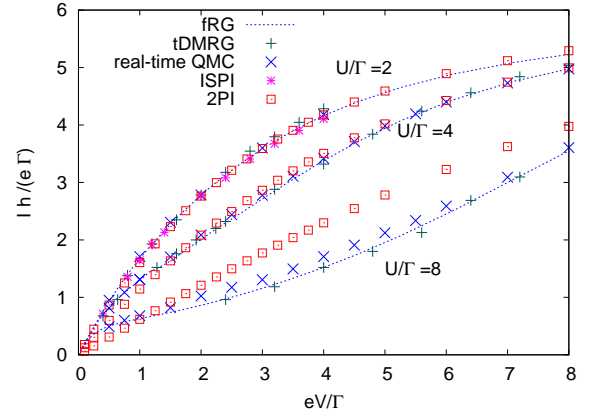


Figure 9: Comparison of the results obtained with different methods, at the symmetric point  $E_0 = -U/2$ . The stationary current is shown as a function of the bias voltage for several coupling strengths. The 2PI and the ISPI methods use  $T = 0.1\Gamma$ .

gion, the 2PI method gives reliable results irrespective of the bias voltage and the temperature, both at the symmetric point ( $E_0 = -U/2$ ) and in the mixed-valence regime.

## B. Effective coupling for $s$ -channel resummation

We close this section with an analysis of the effect of the  $s$ -channel resummation on the effective coupling strength on the dot. This resummation allows us to write the equation for

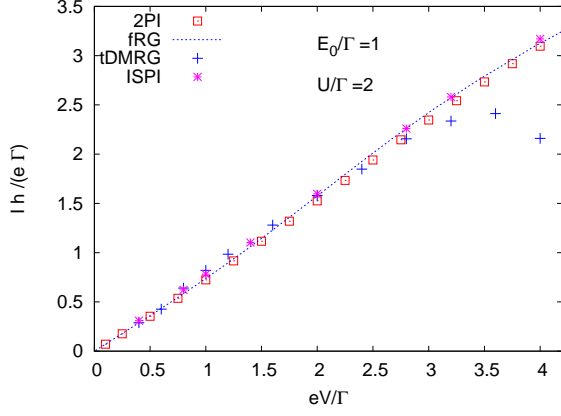


Figure 10: The stationary current in the mixed-valence regime for the coupling of  $U = 2\Gamma$ , and  $E_0 = \Gamma$ . See Ref. [31] of a detailed discussion of the other methods.

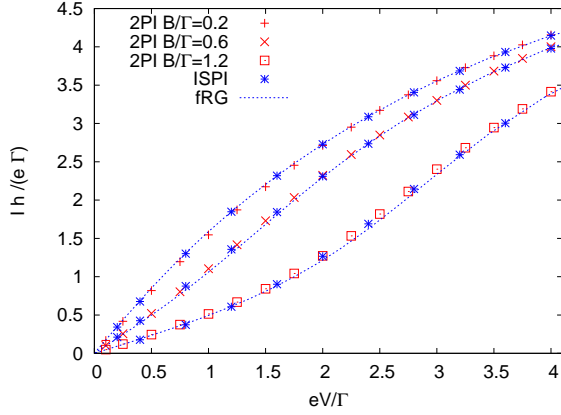


Figure 11: The stationary current as a function of the bias voltage, for several magnetic field strengths.

the fermion self-energy as

$$\begin{aligned}\Sigma^F &= U(FA^F - \frac{1}{4}\rho A^\rho) = UU_{\text{eff}}(F\Pi^F - \frac{1}{4}\rho\Pi^\rho), \\ \Sigma^\rho &= U(\rho A^F + FA^\rho) = UU_{\text{eff}}(\rho\Pi^F + F\Pi^\rho).\end{aligned}\quad (56)$$

where

$$U_{\text{eff}}(\omega) = \frac{1 - |\Pi^R|^2}{|(\Pi^R)^2 - 1|^2}. \quad (57)$$

is a real,  $\omega$ -dependent effective coupling function. Details of its derivation are given in Appendix D.

Note that, before resummation,  $\Sigma^F$  and  $\Sigma^\rho$  had the same form, with  $U_{\text{eff}}$  replaced by  $U$ , see in Eqs. (23) and (C2). The time arguments in (56) are always  $(t, t')$ .

One can thus understand the effect of the resummation as introducing a frequency dependent 4-point vertex. This vertex only depends on one frequency, because only the  $s$ -channel diagrams are resummed. In Fig. 13 we show the effective cou-

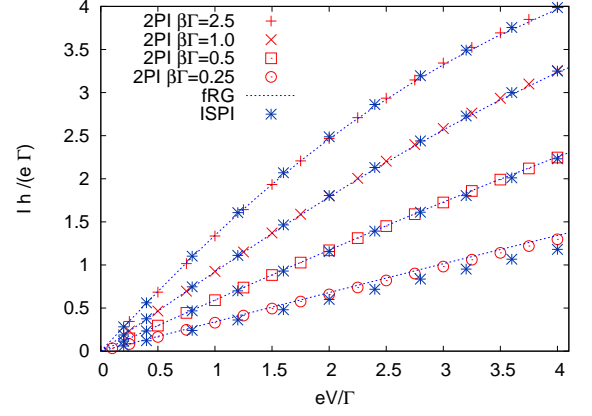


Figure 12: The stationary current is plotted as a function of the bias voltage for several temperatures.

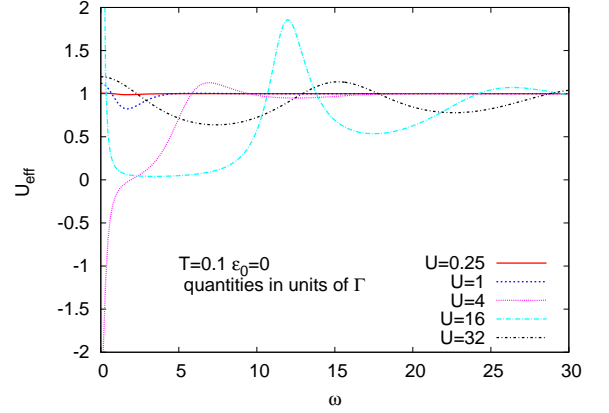


Figure 13: The effective coupling for various couplings as a function of the frequency.

pling for various bare couplings  $U$ . For small couplings, one has  $U_{\text{eff}} \approx 1$  because  $\Pi$  is proportional to the coupling  $U$ . For medium-sized  $U$ , the effective coupling shows big deviations from 1, and for large  $U$  the effective coupling again approaches one.

## VII. CONCLUSIONS

In this paper we have studied the real-time evolution of the Anderson quantum dot, using the two-particle-irreducible (2PI) effective-action approach. The dynamical evolution of correlation functions is described by Kadanoff-Baym equations of motion derived from the effective action in nonperturbative approximation. Two different approximations were considered: the second-order (sunset) coupling-expansion approximation and the  $s$ -channel resummation approximation, in which the bubble chains (bubbles with equal-spin propagators, alternating spins in adjacent bubbles) were summed to all orders.

The leads were taken into account by integrating them out exactly, using a grand-canonical initial density matrix. At nonzero bare interaction strength  $U$  of the dot fermions we compared our results with those obtained within different other approaches. At moderate couplings, the 2PI method gives reliable results irrespective of the temperature or the bias voltage both in the particle-hole symmetric and the mixed valence regimes.

Considering the effective coupling one finds that the resummation can be thought of as using a frequency dependent four point vertex. One way to go beyond the approximations of this study is to take into account a higher loop expansion of the 2PI part  $\Gamma_2[D]$  of the Hubbard-Stratonovich transformed theory. While this requires more numerical effort, since the self energies in higher loop approximation include at least one inner vertex, for which an integration has to be carried out, it is nevertheless possible with current computers.

An expansion of the presented scheme to the non-equilibrium RG approach put forward in Refs. [16, 17] is under development. It was shown that in the  $s$ -channel truncation this RG scheme is equivalent to the 2PI scheme used in this work. Beyond this one can take into account resummations also in the  $t$  and  $u$  channels, also called spin-singlet or electron-hole and electron-electron channels, respectively, which are expected to yield the Kondo-resonance behaviour for large  $U$  [21–23].

### Acknowledgments

The authors would like to thank J. Berges, T. Enss, F. Heindrich-Meisner, S. Jakobs, and H. Schöller for inspiring and useful discussions, J. Eckel for providing the data published in Ref. [34]. They acknowledge the support by the Deutsche Forschungsgemeinschaft, as well as the support by the Alliance Programme of the Helmholtz Association (HA216/EMMI), and by the Excellence Programme FRON-TIER of the University of Heidelberg. A large part of the numerical calculations for this project were done on the bwGRiD (<http://www.bw-grid.de>), member of the German D-Grid initiative, funded by BMBF and MWFK Baden-Württemberg.

### Appendix A: Equal-time propagator

The one-loop contribution to the self-energy gives the mean-field approximation (20) of the dynamic equations (16). Note that  $D_\sigma(t, t')$  has a jump at equal time arguments. Hence and one has the choice between  $D_{-\sigma}(t, t + \epsilon)$  and  $D_{-\sigma}(t, t - \epsilon)$ , or some linear combination of them.

$$\begin{aligned} \lim_{\epsilon \rightarrow +0} D_\sigma(t, t - \epsilon) &= d_\sigma(t) d_\sigma^\dagger(t) = 1 - n_\sigma(t), \\ \lim_{\epsilon \rightarrow +0} D_\sigma(t, t + \epsilon) &= -d_\sigma^\dagger(t) d_\sigma(t) = -n_\sigma(t) \end{aligned} \quad (\text{A1})$$

It is well known that this ambiguity in the 2 point correlation function corresponds to different orderings in the operator language. For example, choosing the second possibility in (A1)

corresponds to the operator Hamiltonian

$$H = \sum_\sigma E_{0\sigma} d_\sigma^\dagger d_\sigma + U d_\uparrow^\dagger d_\uparrow d_\downarrow^\dagger d_\downarrow. \quad (\text{A2})$$

This can be shown by using the fact that a symmetrically ordered Hamiltonian corresponds to a symmetrised path integral prescription. Thus,

$$\begin{aligned} H_{\text{symm}} &= \sum_\sigma E_{0\sigma} d_\sigma^\dagger d_\sigma + \frac{U}{4} (d_\uparrow^\dagger d_\uparrow d_\downarrow^\dagger d_\downarrow - d_\uparrow^\dagger d_\uparrow d_\downarrow^\dagger d_\downarrow \\ &\quad + d_\uparrow^\dagger d_\uparrow d_\downarrow^\dagger d_\downarrow - d_\uparrow^\dagger d_\uparrow d_\downarrow^\dagger d_\downarrow) \\ &= \sum_\sigma \left( E_{0\sigma} - \frac{U}{2} \right) d_\sigma^\dagger d_\sigma + U d_\uparrow^\dagger d_\uparrow d_\downarrow^\dagger d_\downarrow. \end{aligned} \quad (\text{A3})$$

is related to

$$\begin{aligned} \Sigma_{\text{symm}, \sigma}^{MF} &= \frac{1}{2} \left[ \lim_{\epsilon \rightarrow +0} D_{-\sigma}(t, t - \epsilon) + \lim_{\epsilon \rightarrow +0} D_{-\sigma}(t, t + \epsilon) \right] \\ &= \frac{1}{2} - n_{-\sigma} = F_{-\sigma}(t, t). \end{aligned} \quad (\text{A4})$$

By analyzing the equations of motion, one finds that this is equivalent to using the original Hamiltonian (A2), and the following prescription

$$\begin{aligned} \Sigma_\sigma^{MF}(t, t') &= iU \delta(t - t') \lim_{\epsilon \rightarrow +0} D_{-\sigma}(t, t + \epsilon) \\ &= -iU n_{-\sigma} \delta(t - t'). \end{aligned} \quad (\text{A5})$$

For higher-order contributions no such complication of ordering is present.

### Appendix B: Numerical Implementation

The naive (Euler) discretisation of the equation (B1) breaks down quickly, because the absolute value of  $F(t, t')$  is not conserved, even for zero right-hand side  $R$ .

$$(i\partial_t - E_0)F(t, t') = R \quad (\text{B1})$$

One gets a much better discretisation if one first inserts an ansatz which describes the free behaviour, and then discretises the equation for the remaining time evolution.

For this one introduces the new functions  $H(t, t')$  and  $s(t, t')$

$$F(t, t') = e^{-iE_0(t-t')} H(t, t'), \quad \rho(t, t') = e^{-iE_0(t-t')} s(t, t'). \quad (\text{B2})$$

Without interactions, the solution is  $H(t, t') = \text{const}$  and  $s(t, t') = \text{const}$ . Writing the discretised equations for  $H(t, t')$ , and similarly for  $s(t, t')$ :

$$H(t + \Delta t, t') = -ie^{iE_0(t-t')} R H(t, t') \Delta t + H(t, t'), \quad (\text{B3})$$

and multiplying this equation with  $e^{-iE_0(t+\Delta t-t')}$  one gets an equation for  $F(t, t')$ :

$$F(t + \Delta t, t') = -ie^{-iE_0 \Delta t} R \Delta t + F(t, t') e^{-iE_0 \Delta t}. \quad (\text{B4})$$

This equation defines a discretisation of (B1) that is different from the usual Euler discretisation, but has the same continuum limit. We see that using this algorithm, the free evolution is reproduced without numerical errors. Hence for a moderate right-hand side one can use a big timestep, and still conserve the unitarity of the equation to a good degree.

Solving the 2PI equations, we set  $\rho(t, t) = i$  explicitly, as prescribed by the anticommutation relations. Everything else is calculated using the discretisation (B4) of the EOM. On the right-hand side of the EOM, the memory integrals for a particular time  $t$  require field values in the past, which have been computed before. Therefore, our scheme allows an explicit calculation of the next timestep from known quantities. We typically use  $\Delta t = 0.01 - 0.02$ , which gives the continuum limit to a good accuracy.

For zero magnetic field, when  $E_{0\uparrow} = E_{0\downarrow}$ , one can use a symmetric initial condition to save numerical resources. These symmetries apply in the second order truncation as well as in the resummed truncation. We discuss the resummed equations below: starting from an initial condition, where the following equations are satisfied for  $t = t' = 0$ , then they hold for any  $t, t' > 0$ .

$$\begin{aligned}\bar{G}_{21}(t, t') &= \bar{G}_{12}(t', t), & \bar{G}_{11}(t, t') &= \bar{G}_{22}(t, t'), \\ \Pi_{11}(t, t') &= \Pi_{22}(t, t'), & D_{\uparrow}(t, t') &= D_{\downarrow}(t, t').\end{aligned}\quad (\text{B5})$$

The real constraint set by these equations is only  $D_{\uparrow}(0, 0) = D_{\downarrow}(0, 0)$ , the rest follows automatically via the constraint equations (31) of the scalar fields and the EOM for the fermionic fields.

### Appendix C: Decomposition of the propagator $G$

According to (31),  $G(t, t')$  is decomposed as  $G(t, t') = \bar{G}(t, t') + iU\sigma_1\delta(t - t')$ , where  $\sigma_1$  is the first Pauli matrix. The equation for  $\bar{G}$  reads

$$\begin{pmatrix} \bar{G}_{21} & \bar{G}_{22} \\ \bar{G}_{11} & \bar{G}_{12} \end{pmatrix} = iU\Pi * \bar{G} - U^2 \begin{pmatrix} \Pi_{12} & \Pi_{11} \\ \Pi_{22} & \Pi_{21} \end{pmatrix}. \quad (\text{C1})$$

The fermionic and bosonic self energies can be decomposed in the usual way into  $F$  and  $\rho$  parts

$$\begin{aligned}\Sigma_{\sigma}^F &= -1(F_{\sigma}\bar{G}_{F\sigma\sigma} - \frac{1}{4}\rho_{\sigma}\bar{G}_{\rho\sigma\sigma}), \\ \Sigma_{\sigma}^{\rho} &= -1(\rho_{\sigma}\bar{G}_{F\sigma\sigma} + F_{\sigma}\bar{G}_{\rho\sigma\sigma}), \\ \Pi_{\sigma}^F &= |F_{\sigma}|^2 - \frac{1}{4}|\rho_{\sigma}|^2, \\ \Pi_{\sigma}^{\rho} &= 2\text{Re}(F_{\sigma}^*\rho_{\sigma}),\end{aligned}\quad (\text{C2})$$

where, similar to the fermions, the scalar propagator is decomposed into

$$\bar{G}_{ij}(t, t') = \bar{G}_{ij}^F(t, t') - \frac{i}{2}\text{sign}_C(t - t')\bar{G}_{ij}^{\rho}(t, t'). \quad (\text{C3})$$

In this setup, the ordering problem also appears, in the equations for the field average of the  $\chi$  fields. It can be dealt with

similarly as in the previous subsection: symmetric Hamiltonian corresponds to a symmetrised path integral. From this one deduces the prescription for the non-symmetrised Anderson Hamiltonian (1). Eq. (16) corresponds to the ordering of (1) when using

$$M_{\sigma}(t) = E_{0\sigma} + Un_{-\sigma}(t). \quad (\text{C4})$$

The scalar constraint equation (C1) can be decomposed using the identity

$$\begin{aligned}(iA * B)(t, t') &= \int_0^t dz A^{\rho}(t, z) B^F(z, t') \\ &\quad - \int_0^{t'} dz A^F(t, z) B^{\rho}(z, t') \\ &\quad - \frac{i}{2}\text{sign}_C(t - t') \int_{t'}^t A^{\rho}(t, z) B^{\rho}(z, t').\end{aligned}\quad (\text{C5})$$

### Appendix D: Effective coupling for $s$ -channel resummation

In this appendix we give the details of the calculation of the effective coupling given in Section VIB. In the zero-magnetic-field case, where  $E_{0\uparrow} = E_{0\downarrow}$ , and the symmetries of (B5) hold, one can define:

$$\begin{aligned}A(t, t') &= \frac{\bar{G}_{11}(t, t')}{U}, & B(t, t') &= \frac{\bar{G}_{21}(t, t')}{U}, \\ \Pi(t, t') &= U\Pi_{11}(t, t').\end{aligned}\quad (\text{D1})$$

Hence, the constraint equations (31) can be written as (suppressing time arguments)

$$A = i\Pi * B - \Pi, \quad B = i\Pi * A. \quad (\text{D2})$$

After the transient processes are finished, in the stationary state, all two-point functions will only depend on the differences of the time coordinates. In this case we can push the initial time to negative infinity, and we can use the following decomposition identities for convolution on the Schwinger-Keldysh contour starting at  $t_0 = -\infty$ :

$$\begin{aligned}i(X * Y)^F &= X^R * Y^F - X^F * Y^A, \\ i(X * Y)^{\rho} &= X^R * Y^{\rho} - X^{\rho} * Y^A, \\ i(X * Y)^R &= X^R * Y^R, \\ i(X * Y)^A &= -X^A * Y^A\end{aligned}\quad (\text{D3})$$

where the retarded and advanced two-point functions are defined as

$$\begin{aligned}G^R(t, t') &= \theta(t - t')G^{\rho}(t, t'), \\ G^A(t, t') &= \theta(t' - t)G^{\rho}(t, t').\end{aligned}\quad (\text{D4})$$

Using this in Eq. (D2), after eliminating  $B$  and Fourier transformation with respect to  $t - t'$ , we obtain

$$\begin{aligned}A^F &= \Pi^R \Pi^R A^F - \Pi^R \Pi^F A^A - \Pi^F + \Pi^F \Pi^A A^A, \\ A^{\rho} &= \Pi^R \Pi^R A^{\rho} - \Pi^R \Pi^{\rho} A^A - \Pi^{\rho} + \Pi^{\rho} \Pi^A A^A\end{aligned}\quad (\text{D5})$$

where we have omitted arguments ( $\omega$ ). With the help of (D3), Eq. (D2) can be rewritten as

$$(1 + \Pi^R A^A - \Pi^A A^A)(\Pi^A \Pi^A - 1) = \Pi^R \Pi^A - 1. \quad (\text{D6})$$

We can write

$$A^P = -\Pi^P U_{\text{eff}}, \quad A^F = -\Pi^F U_{\text{eff}} \quad (\text{D7})$$

where

$$U_{\text{eff}}(\omega) = \frac{1 - \Pi^R \Pi^A}{((\Pi^R)^2 - 1)(\Pi^A)^2 - 1) = \frac{1 - |\Pi^R|^2}{|(\Pi^R)^2 - 1|^2}. \quad (\text{D8})$$

which is the expression given in Eq. (57).

- 
- [1] G. Cuniberti, G. Fagas, and K. Richter, eds., *Introducing Molecular Electronics* (Springer, Heidelberg, 2005).
  - [2] J. Reichert, R. Ochs, D. Beckmann, H. B. Weber, M. Mayor, and H. v. Löhneysen, Phys. Rev. Lett. **88**, 176804 (2002).
  - [3] R. H. M. Smit, Y. Noat, C. Untiedt, N. D. Lang, M. C. van Hemert, and J. M. van Ruitenbeek, Nature **419**, 906 (2002).
  - [4] H. Park, J. Park, A. K. L. Lim, E. H. Anderson, A. P. Alivisatos, and P. L. McEuen, Nature **407**, 57 (2000).
  - [5] M. Galperin, M. A. Ratner, and A. Nitzan, Jour. Phys.: Cond. Mat. **19**, 103201 (2007).
  - [6] A. Oguri, Phys. Rev. B **64**, 153305 (2001).
  - [7] R. M. Konik, H. Saleur, and A. Ludwig, Phys. Rev. B **66**, 125304 (2002).
  - [8] N. S. Wingreen and Y. Meir, Phys. Rev. B **49**, 11040 (1994).
  - [9] H. Schoeller and J. König, Phys. Rev. Lett. **84**, 3686 (2000).
  - [10] A. Kaminski, Y. V. Nazarov, and L. I. Glazman, Phys. Rev. B **62**, 8154 (2000).
  - [11] A. Rosch, J. Kroha, and P. Wölfle, Phys. Rev. Lett. **87**, 156802 (2001).
  - [12] A. Rosch, J. Paaske, J. Kroha, and P. Wölfle, Phys. Rev. Lett. **90**, 076804 (2003).
  - [13] S. Andergassen, T. Enss, and V. Meden, Phys. Rev. B **73**, 153308 (2006).
  - [14] R. Gezzi, T. Pruschke, and V. Meden, Phys. Rev. B **75**, 045324 (2007).
  - [15] S. G. Jakobs, V. Meden, and H. Schoeller, Phys. Rev. Lett. **99**, 150603 (2007).
  - [16] T. Gasenzer and J. M. Pawłowski, Phys. Lett. **B670**, 135 (2008).
  - [17] T. Gasenzer, S. Keßler, and J. M. Pawłowski, Eur. Phys. Jour. C **70**, 423 (2010).
  - [18] S. G. Jakobs, M. Pletyukhov, and H. Schoeller, Phys. Rev. B **81**, 195109 (2010).
  - [19] C. Karrasch, M. Pletyukhov, L. Borda, and V. Meden, Phys. Rev. B **81**, 125122 (2010).
  - [20] V. Janiš, Phys. Rev. B **60**, 11345 (1999).
  - [21] V. Janiš and P. Augustinský, Phys. Rev. B **75**, 165108 (2007).
  - [22] V. Janiš and P. Augustinský, Phys. Rev. B **77**, 085106 (2008).
  - [23] P. Augustinský and V. Janiš (2010), arXiv:1008.3498.
  - [24] F. B. Anders and A. Schiller, Phys. Rev. Lett. **95**, 196801 (2005).
  - [25] F. B. Anders and A. Schiller, Phys. Rev. B **74**, 245113 (2006).
  - [26] D. Roosen, M. R. Wegewijs, and W. Hofstetter, Phys. Rev. Lett. **100**, 087201 (2008).
  - [27] S. Schmitt and F. B. Anders, Phys. Rev. B **81**, 165106 (2010).
  - [28] R. Egger, L. Mühlbacher, and C. H. Mak, Phys. Rev. E **61**, 5961 (2000).
  - [29] A. J. Daley, C. Kollath, U. Schollwöck, and G. Vidal, Journal of Statistical Mechanics: Theory and Experiment **2004**, P04005 (2004).
  - [30] S. R. White and A. E. Feiguin, Phys. Rev. Lett. **93**, 076401 (2004).
  - [31] F. Heidrich-Meisner, A. E. Feiguin, and E. Dagotto, Phys. Rev. B **79**, 235336 (2009).
  - [32] E. Boulat, H. Saleur, and P. Schmitteckert, Phys. Rev. Lett. **101**, 140601 (2008).
  - [33] S. Weiss, J. Eckel, M. Thorwart, and R. Egger, Phys. Rev. B **77**, 195316 (2008).
  - [34] J. Eckel, F. Heidrich-Meisner, S. Jakobs, M. Thorwart, M. Pletyukhov, and R. Egger, New. J. Phys. **12**, 043042 (2010).
  - [35] J. M. Luttinger and J. C. Ward, Phys. Rev. **118**, 1417 (1960).
  - [36] G. Baym, Phys. Rev. **127**, 1391 (1962).
  - [37] J. M. Cornwall, R. Jackiw, and E. Tomboulis, Phys. Rev. D **10**, 2428 (1974).
  - [38] J. Berges, Nucl. Phys. **A699**, 847 (2002).
  - [39] J. Berges, S. Borsányi, and J. Serreau, Nucl. Phys. **B660**, 51 (2003).
  - [40] T. Gasenzer, J. Berges, M. G. Schmidt, and M. Seco, Phys. Rev. **A72**, 063604 (2005).
  - [41] A. Arrizabalaga, J. Smit, and A. Tranberg, Phys. Rev. **D72**, 025014 (2005).
  - [42] J. Berges and T. Gasenzer, Phys. Rev. **A76**, 033604 (2007).
  - [43] M. Kronenwett and T. Gasenzer (2010), arXiv:1006.3330.
  - [44] A. Giraud and J. Serreau, Phys. Rev. Lett. **104**, 230405 (2010).
  - [45] L. V. Keldysh, [Sov. Phys. JETP **20**, 1018 (1965)] Zh. Eksp. Teor. Fiz. **47**, 1515 (1964).
  - [46] K.-C. Chou, Z.-B. Su, B.-L. Hao, and L. Yu, Phys. Rept. **118**, 1 (1985).
  - [47] J. Berges and J. Cox, Phys. Lett. **B517**, 369 (2001).
  - [48] J. Berges, AIP Conf. Proc. **739**, 3 (2005) arXiv:hep-ph/0409233.
  - [49] G. Aarts, D. Ahrensmeier, R. Baier, J. Berges, and J. Serreau, Phys. Rev. D **66**, 045008 (2002).
  - [50] A. M. Rey, B. L. Hu, E. Calzetta, A. Roura, and C. W. Clark, Phys. Rev. A **69**, 033610 (2004).
  - [51] G. Aarts and A. Tranberg, Phys. Rev. **D74**, 025004 (2006).
  - [52] L. Dell'Anna, A. Zazunov, and R. Egger, Phys. Rev. B **77**, 104525 (2008).